ELSEVIER

Coordination Chemistry Reviews 226 (2002) 39–49

COORDINATION CHEMISTRY REVIEWS

www.elsevier.com/locate/ccr

Time resolved spectroscopic studies relevant to reactive intermediates in homogeneous catalysis. The migratory insertion reaction

Peter C. Ford *, Steve Massick

Department of Chemistry and Biochemistry, University of California, Santa Barbara, CA 93106-9510, USA

Received 3 April 2001; accepted 21 September 2001

Contents

Abstract

A major challenge of mechanistic organometallic chemistry is to characterize the structure and dynamics of reactive intermediates in stoichiometric and catalytic processes. In this context, time resolved spectroscopic techniques can be used to investigate reactive intermediates generated by laser flash photolysis of suitable organometallic precursors. Specific examples will be drawn from ongoing mechanistic research in these laboratories in which time-resolved infrared (TRIR) and time-resolved optical (TRO) detection are used to probe the reactivities and structures of intermediates in the carbonylations of metal–alkyl bonds, a key pathway in catalytic activation of carbon monoxide. The principal focus will be upon the migratory insertion mechanisms of cobalt carbonyl complexes similar to those used in alkene hydroformylation catalysis as well as model systems based on manganese carbonyls.

Keywords: Carbonylations; Carbon monoxide; Catalytic activation

1. Introduction

Organometallic reactions important to homogenous catalysis schemes include the activation of C–H and H–H bonds, ligand substitution, carbon monoxide migratory insertions, alkene isomerization and oligomerization etc. [1,2]. A major goal in elucidating the detailed mechanisms is to characterize the structures and reactivities of intermediates formed along reaction coordinates. Such transients are elusive under catalytic conditions owing to low steady state concentrations. A strategy used in this laboratory has been to prepare non-steady state concentrations of such intermediates by laser flash photolysis of suitable precursors [3–16].

* Corresponding author. Tel.: +1-805-8932443; fax: +1-805-8934120.

E-mail address: ford@chem.ucsb.edu (P.C. Ford).

0010-8545/02/$ - see front matter
PII: S0010-8545(01)00443-X

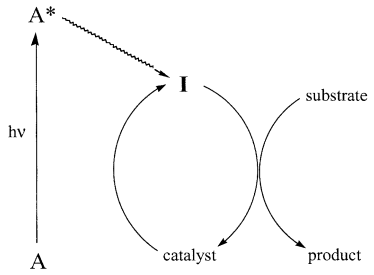

Fig. 1. Cartoon illustrating the photochemical techniques to generate non-steady state concentrations of reactive intermediates for a catalytic cycle by flash photolysis of a suitable precursor **A**.

Fig. 1 is a cartoon illustrating this strategy. Once these short-lived transients are generated, they can be interrogated with time-resolved optical (TRO) or time-resolved infrared (TRIR) spectral techniques, which provide an ensemble of spectroscopic and dynamic information. Instrumentation developed in this laboratory provides the opportunity to carry out these reactions at elevated temperatures and pressures relevant to industrial catalysis conditions [13].

What types of intermediates might one expect to be able to prepare and detect in this manner? For many metal complexes, the most common photoreaction would be simple ligand dissociation (Eq. 1), since the M–L bonds are usually the weakest in the complex. With molecular ligands such as CO or an alkene, dissociation is heterolytic, but with metal alkyls and similar

$$RML_n \xrightarrow{h\nu} \begin{cases} \xrightarrow{(a)} RML_{n-1} + L \\ \xrightarrow{(b)} R^{\bullet} + ML_n \end{cases} \quad (1)$$

species, homolytic dissociation to radicals is common. In solution, other relaxation processes are sufficiently fast that one normally expects but a single ligand to be labilized, although in the gas phase, multiple dissociations are common.

2. Time resolved spectroscopic techniques

2.1. Apparatus

Most flash photolysis studies involving the measurement of transient absorption behavior of organometallic intermediates are carried out on apparatus with a standard 'pump-probe' configuration as illustrated in Fig. 2. At UCSB, our studies have largely been carried out in the ns–ms regime, where continuous IR or UV–vis sources can be used as probes. The pump source is either a XeCl Excimer laser (308 nm) or a Nd/YAG laser operating at the second (532 nm), third (355 nm) or fourth harmonic (266 nm). For time resolved optical (TRO) detection the UV–vis probe source is a xenon short arc lamp. For kinetics studies, the light from this is passed through a monochromator to give a (variable) single frequency source, which is detected using a PMT. Alternatively, the full visible range spectrum can be recorded using a spectrograph and a CCD camera, with the timing defined by electronic gating.

TRIR detection is attractive for kinetic studies of organometallic reactions, especially if the relevant reactants, intermediates, and/or products include groups, such as carbonyls, which are strong IR chromophores. The, UV–vis absorptions for many organometallic compounds in solution are generally broad and featureless, and bands of the various species often overlap. IR spectra tend to give much better resolution between individual species, and the relatively narrow and sometimes structure specific bands often allow for direct observation of the temporal decay and appearance of individual species without interference from excessive overlapping. Kinetics studies at UCSB with IR detection were explored at (variable) single probe frequencies using a tunable IR laser source and a fast rise time solid state detector. Some experiments reviewed here in-

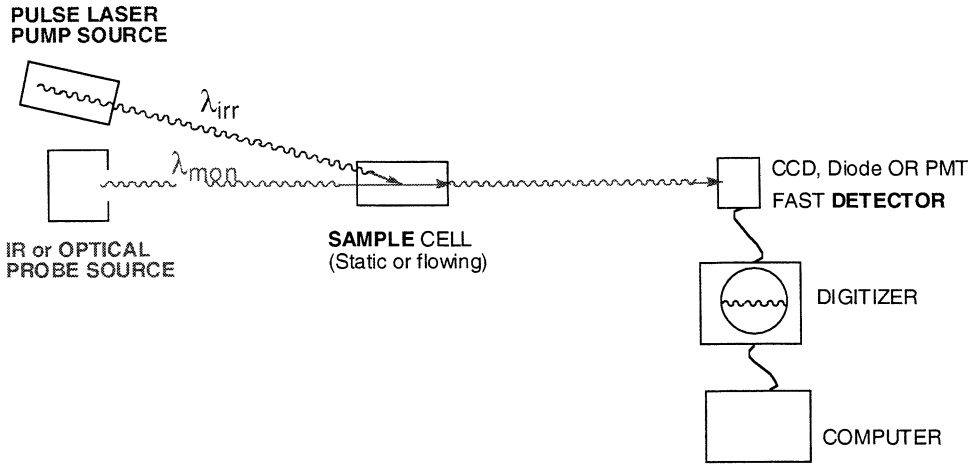

Fig. 2. Generic pump-probe apparatus for time resolved optical or infrared studies.

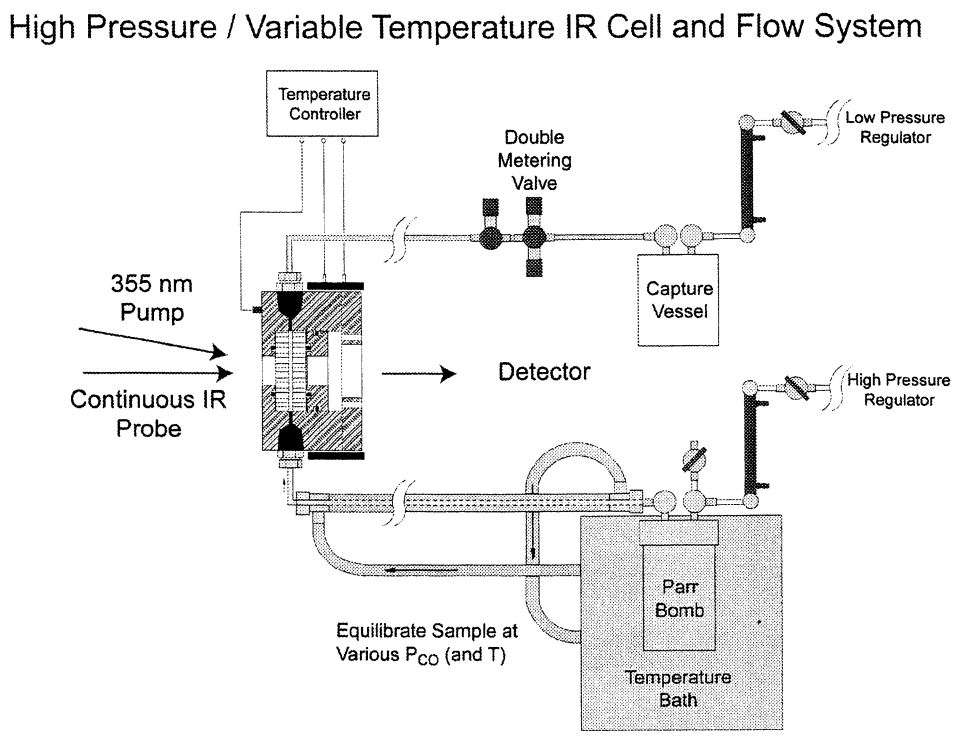

Fig. 3. HP/VT flow cell for TRIR studies.

volved step-scan FTIR techniques on an instrument at Los Alamos National Laboratory. The general makeup of various TRIR systems has been reviewed [16], and several other laboratories have used TRIR spectroscopic techniques extensively for studying the photoreactions of organometallic compounds [17–19].

It is generally necessary to carry out considerable signal averaging to assure reasonably large signal to noise (s/n) ratios, and this requires multiple laser pulsing of the sample. Thus, it is generally desirable to have the sample flowing through the excitation region at a pace such that physical motion is slow relative to the observation time, but sufficiently rapid for sample renewal between laser pulses. It is also desirable to define and control the reaction conditions (temperature, gaseous atmosphere, etc.). In this context, the high pressure/variable temperature (HP/VT) flow system custom built for these studies [13] is designed to operate under gaseous pressures to 100 atm and temperatures upto 150 °C, in order to approach conditions more relevant to certain known industrial catalysts. This is illustrated in Fig. 3.

2.2. An example: intermediates in the flash photolysis of $Mn(CO)_5CH_3$

Characterization of a reactive organometallic intermediate by TRIR technique is illustrated with the manganese carbonyl complex $Mn(CO)_5CH_3$ ($\mathbf{M}_{Mn}$) [8]. Fig. 4 shows the TRIR spectrum resulting from the flash photolysis of $\mathbf{M}_{Mn}$ in cyclohexane solution under CO. The notable features are the prompt formation of a transient species **X**, with new ν_{CO} absorptions at 1992, 1986 and 1952 cm^{-1}, which decay exponentially (k_{obs}) within a few μs. A plot of k_{obs} versus [CO] proved to be linear with slope k_{CO} of 4.5×10^8 M^{-1} s^{-1} (295 K) and a zero intercept consistent with the rate law in Eq. (2). Reformation of $\mathbf{M}_{Mn}$ occurred at the same rate (although some permanent bleaching was observed owing to competing photochemical cleavage of the Mn–Me bond).

$$-\frac{d[\mathbf{X}]}{dt} = k_{obs}[\mathbf{X}] = k_{CO}[CO][\mathbf{X}] \quad (2)$$

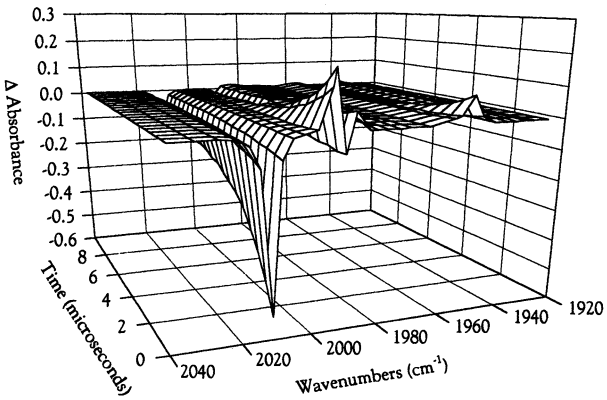

Fig. 4. TRIR spectral data resulting from 308 nm flash photolysis of $Mn(CO)_5CH_3$ in 295 K cyclohexane under 10% CO (0.001 M).

Table 1
Rate constants for CO addition (k_{CO}) and methyl migration (k_M) reactions of $\mathbf{I}_{Mn}$ in various solvents determined from optical flash photolysis experiments

Solvent	k_{CO} (M^{-1} s^{-1})	k_M (s^{-1})	k_{CO} for **X** (M^{-1} s^{-1})[b]
PFMC	1.5×10^4	<1.0	$\sim1\times10^{10}$
Benzene	3.3×10^3	6.7	
Cyclohexane	6.5×10^3	9.0	4.5×10^8
Dichloromethane	5.3×10^3	30	
1,2 Dichloroethane	7.0×10^3	47	
THF	$<5\times10^2$	8.8	1.4×10^2

Data from Ref. [9].

The TRIR spectra of **X** displayed a marked dependence on the nature of the solvent medium; for example, in tetrahydrofuran, the ν_{CO} bands appeared at lower frequency (1974, 1964 and 1921 cm^{-1}), than in cyclohexane. Furthermore, k_{CO} proved to be strongly solvent dependent, ranging from $\sim10^{10}$ M^{-1} s^{-1} in perfluoromethylcyclohexane (PFMC) solution to 1.4×10^2 M^{-1} s^{-1} in THF, nearly eight orders of magnitude smaller. Thus, the spectra and dynamics of the intermediates observed upon photo dissociation of CO from $Mn(CO)_5CH_3$ was attributed to the solvento species *cis*-$Mn(CO)_4(Sol)CH_3$, which react with CO to regenerate $\mathbf{M}_{Mn}$ (Eq. (3))[8].

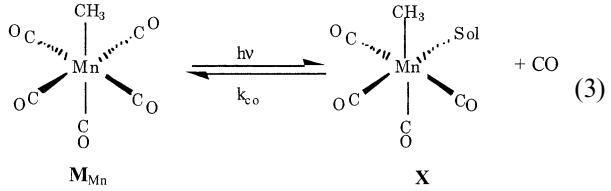

$\mathbf{M}_{Mn}$ **X** (3)

3. Mechanisms of CO migratory insertion into metal alkyl bonds

Carbon monoxide 'migratory insertion' into metal alkyl bonds is the key carbon–carbon bond formation pathway in catalytic carbonylations such as acetic acid synthesis from methanol, alkene hydroformylations, etc. [1,2]. Alkyl manganese carbonyl complexes such as $\mathbf{M}_{Mn}$ have been extensively probed as mechanistic models for this fundamental important class of organometallic reactions [20]. Such studies suggest that alkyl migration to a *cis* carbonyl leads to a reactive intermediate ($\mathbf{I}_{th}$) in a step promoted by more polar solvents. Trapping of $\mathbf{I}_{th}$ by a ligand completes the process, although a concerted reaction may function in some cases.

Our strategy for characterizing the structure and reactivity of potential intermediates starts with an acyl complex, i.e. the product of the thermal reaction. Photodissociation of a ligand L′ from the acyl complex **A** prepares a reactive intermediate **I** (e.g. Eq. (4)) with the same composition as proposed for $\mathbf{I}_{th}$. Time resolved spectroscopic studies are then used to interrogate the nature of **I** as well as the dynamics of the reactions with various L′ to give the stable acyl products and of reverse alkyl migration to give the metal alkyl complex **M**.

The resulting TRO and TRIR spectra as well as the reaction kinetics under various conditions are

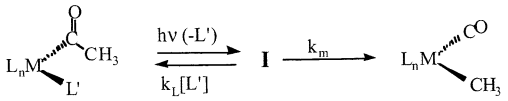

(4)

then interpreted in terms of potential mechanisms. Comparisons with the rates obtained for **I** in this manner to the competitive reactivities deduced for $\mathbf{I}_{th}$ based on steady state kinetics methods can further be employed to analyze whether **I** serves as a reasonable model for $\mathbf{I}_{th}$. The majority of our studies to date have been with the model systems $Mn(CO)_5(C(O)R)$ and $(\eta^5\text{-}C_5H_5)Fe(CO)(C(O)R)$ [6–9,11–13], but ongoing studies are probing analogous intermediates generated from known cobalt [14] and rhodium catalysts [21] under conditions more relevant to a catalytic medium.

3.1. Manganese carbonyl complexes

The IR spectrum of $Mn(CO)_5(C(O)CH_3)$ ($\mathbf{A}_{Mn}$) displays carbonyl stretching bands at 2110, 2051, 2012(vs.) and 1661(acyl) cm^{-1}, that are essentially independent of the solvent medium. Flash photolysis of $\mathbf{A}_{Mn}$ in cyclohexane (296 K) generates a transient with ν_{CO} bands at 1990, 1952, 1606 (w) cm^{-1} [9]. A similar spectrum (ν_{CO} bands 2080 (w), 1998, 1941, 1607 (w) cm^{-1}) was observed for $\mathbf{I}_{Mn}$ upon photolysis of $\mathbf{A}_{Mn}$ in a methylcyclohexane glass at 196 K. The TRIR spectrum of $\mathbf{I}_{Mn}$ displayed moderate sensitivity to solvent (e.g. in tetrahydrofuran (THF), ν_{CO} bands appeared at 1981 (br) and 1931 (br) cm^{-1}), but the effect was considerably smaller than was seen above in the flash photolysis of $\mathbf{M}_{Mn}$. More dramatically, the dynamic behavior of $\mathbf{I}_{Mn}$ was very different from that of **X**. Although, $\mathbf{I}_{Mn}$ reacted with CO to regenerate $\mathbf{A}_{Mn}$, the rate of this reaction in cyclohexane was orders of magnitude slower ($k_{CO}=65\times10^3$ M^{-1} s^{-1} in 296 K cyclohexane) than the analogous reaction of **X** to regenerate **M** under analogous conditions (8.5×10^8 M^{-1} s^{-1}). Furthermore, the k_{CO} values for $\mathbf{I}_{Mn}$ vary by less than a factor of 5 among the solvents PFMC, cyclohexane, 1,2-dichloroethane and benzene, but drop by more than an order of magnitude in THF (Table 1) [9].

The reaction of $\mathbf{I}_{Mn}$ for which there is no analogy in **X**, is the migration of the methyl group to the metal to form $\mathbf{M}_{Mn}$, which occurs with a unimolecular rate constant (k_M) of 9.0 s^{-1} in 296 K cyclohexane. Unlike k_{CO}, k_M is quite sensitive to the nature of the respective solvents (Table 1) [9].

Electronic excitation of $\mathbf{A}_{Mn}$ initiates photoreactions faster than the ns time resolution of these experiments. While some acetyl–metal bond fragmentation and 'prompt' formation of $\mathbf{M}_{Mn}$ are apparent, the principal pathway is CO dissociation to give $\mathbf{I}_{Mn}$. What form might $\mathbf{I}_{Mn}$ take? Depicted below (L, CO) are some alternatives, notably, the fully unsaturated species **U**, the chelated structure **C** with a η^2-carbonyl group, the solvated intermediate **S** and the bidentate transient **B** with the methyl group in an agostic interaction with the metal center. A truly coordinatively unsaturated intermediate (**U**) of a d^6 metal center such as Mn(I) is unlikely to be seen on the ns–μs time scales of these experiments. Earlier workers have demonstrated that $Cr(CO)_5$ and its Mo and W pentacarbonyl homologs as well as analogously unsaturated species bind

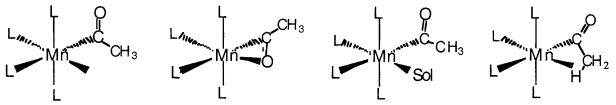

alkanes with dissociation energies as large as 10 kcal M^{-1} and bind stronger donor ligands much more strongly [22]. In the same context, thus, the solvento species **S** must be given serious attention as a possible candidate for $\mathbf{I}_{Mn}$, not only in strongly donor media but also in hydrocarbon solvents. The presence or absence of solvent effects on spectra or reactivities might be used to evaluate the possible role of **S**. Differentiating **B** and **C** may be more challenging, since both agostic and η^2-CO forms of acyl coordination have been shown to be in equilibrium for solutions of the molybdenum acyl complex $Mo(C(O)CH_2SiMe_3)(S_2CNMe_2)(CO)(PMe_3)_2$ and analogs [23]. However, in the case of the manganese complexes, recent DFT calculations suggest that **C** is considerably lower in energy than **B** [24]. The calculations will be discussed further below.

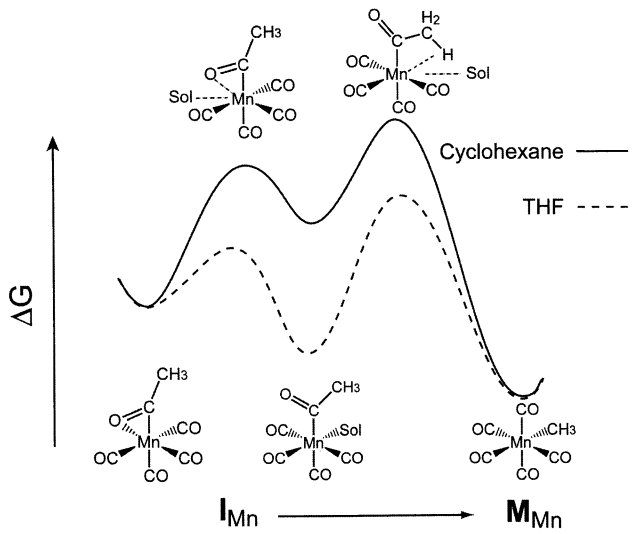

Fig. 5. Free energy profile for the methyl migration pathway of $\mathbf{I}_{Mn}$.

If the L are carbonyls, the ν_{CO} bands are a fairly sensitive probe of the electronic environment at the metal. For **S**, these should shift to lower frequencies as solvent donor strength increases, and the lability of **S** in subsequent reactions with other ligands including CO should decrease as was seen for $Mn(CO)_4(Sol)(CH_3)$ [8]. In contrast, while none of the spectra or kinetics described here are likely to find the bulk solvent a totally innocent player, the spectral and kinetics properties of the **C** or **B** should be but modestly solvent sensitive. In Table 1, kinetics data for the reaction of $\mathbf{I}_{Mn}$ with CO in different solvents [9] are compared with those for **X**. The k_L values in Table 1 show that the k_{CO} values for $\mathbf{I}_{Mn}$ are much less sensitive to solvent as are those of **X**. Furthermore, the comparative sluggishness with which $\mathbf{I}_{Mn}$ undergoes ligand substitution in weakly coordinating solvents relative to **X** suggests that $\mathbf{I}_{Mn}$ is not a solvento species except in stronger donor solvents, where the rates of ligand substitution are similar. Thus, it is our view that the spectral and kinetic data for $\mathbf{I}_{Mn}$ are most consistent with the η^2 chelate **C** in weakly coordinating solvents, but with **S** in more strongly donating solvents.

We now turn to the effect of solvent on the rate of methyl migration, nominally, the microscopic reverse of the first step in the thermal carbonylation reaction. The k_M values in various solvents are summarized in Table 1. Notably, the trends observed for k_M do not parallel those of the ligand substitution reactions. Although, CO reaction with $\mathbf{I}_{Mn}$ is much faster in cyclohexane than in THF, methyl migration rates are nearly identical in the two solvents. The similarity must be coincidental given the different structures in the two solvents. What is remarkable about the data in Table 1 is that the rates of methyl migration increase with relative solvent donor strength for those very media where k_{CO} shows little solvent dependence and it appears that the structure of $\mathbf{I}_{Mn}$ is that of the η^2 chelate **C**.

Fig. 5 offers an explanation of the role of the solvent in promoting methyl migration to form $\mathbf{M}_{Mn}$ from $\mathbf{I}_{Mn}$. In weakly coordinating solvents (alkanes, aromatics, halocarbons), where $\mathbf{I}_{Mn}$ appears to be present as the η^2 chelate **C**, the solvent is nonetheless involved in the methyl migration step owing to the solvent dependence of k_M. Upon inspection of the η^2 acyl structure, it is difficult to imagine a one-step process by which it could rearrange to $\mathbf{M}_{Mn}$. We propose that the trend of in-

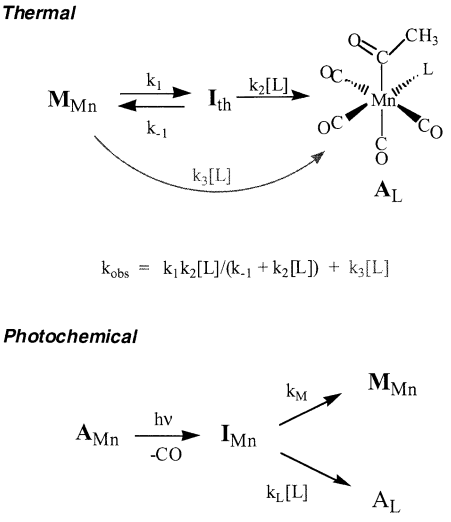

Scheme 1.

creasing k_M with donating ability of the solvent is the result of the η^2 chelate **C** reacting first to form the solvento species, which then undergoes methyl migration with concerted loss of solvent. This is the microscopic reverse of the previously proposed 'solvent assisted' methyl migration. In THF, the lowest energy form $\mathbf{I_{Mn}}$ is already the solvento species **S**. Thus, stabilization of **S** by Mn–THF bonding offsets stabilization of the k_M transition state by solvent–metal interactions, giving the fortuitous similarity of the $\Delta G^{\ddagger}_M$ values in cyclohexane and THF (Fig. 5).

3.1.1. Comparison of the thermal and photochemical kinetics

A crucial question remains to be resolved, is the photochemically generated intermediate, the same as the one produced along the reaction coordinate of the thermal carbonylation under analogous conditions? While data concerning solvent assistance in the above photochemical studies do qualitatively agree with previously observed thermal results, we can make a quantitative comparison of the reactivity of $\mathbf{I}_{Mn}$ and $\mathbf{I}_{th}$. Specifically, if an intermediate shows the same branching selectivity between methyl migration and ligand substitution whether it is produced thermally or photochemically, then the two intermediates are likely to be the same species.

The reaction of $\mathbf{M}_{Mn}$ with $P(OMe)_3$ in THF was investigated in order to provide comparative thermal and photochemical data under closely analogous conditions. Earlier kinetics studies [25] of thermal reactions of $\mathbf{M}_{Mn}$ with various L to give the respective acetyl complexes *cis*-$\mathbf{A}_L$ in various solvents were interpreted in terms of the thermal model illustrated in Scheme 1. In a donor solvent such as THF, the lowest energy pathway is consistent with the formation of the intermediate $\mathbf{I}_{th}$. This would give the relationship $k_{obs} = k_1k_2[L]/(k_{-1} + k_2[L])$ and values of k_1 as well as the ratio k_1/k_2 can be obtained for various L from the slopes and intercepts of double reciprocal k_{obs}^{-1} versus $[L]^{-1}$ plots. Indeed, reaction of $\mathbf{M}_{Mn}$ with excess $P(OMe)_3$ to give *cis*-$CH_3C(O)Mn(CO)_4(P(OMe)_3)$ in THF followed pseudo first order kinetics, and from the linear plot k_{obs}^{-1} versus $[L]^{-1}$, the values $k_1 = (8.5 \pm 0.9) \times 10^{-4}$ s^{-1} and $k_{-1}/k_2 = (6.6 \pm 1.3) \times 10^{-3}$ M [25] were determined.

If $\mathbf{I_{Mn}}$ identified by the photochemical techniques is indeed the same as the thermal intermediate $\mathbf{I}_{th}$, then k_M is k_{-1}, k_L is k_2 and k_{-1}/k_2 should equal k_M/k_L. The photochemical experiment allows one to determine k_M and k_L independently. The calculated k_M/k_L ratio from the photochemical experiment is $(5.5 \pm 1.5) \times 10^{-3}$ M, the same, within experimental uncertainty, as the ratio k_{-1}/k_2 ($(6.6 \pm 1.3) \times 10^{-3}$ M). Thus, the assertion that the photochemically generated intermediates are relevant to thermally induced migratory insertion is supported at least for the reactions in THF.

It is notable that in THF solution, the photochemically generated intermediate $\mathbf{I_{Mn}}$ was concluded to be the solvento species **S**, rather than the η^2-acyl chelate complex **C** found in weakly donor solvents. As discussed above (and in [9]), the latter configuration does not appear to lie on a direct pathway between $\mathbf{M}_{Mn}$ and $\mathbf{A}_{Mn}$. Nonetheless, the sensitivity of the rates of the methyl migration pathway from $\mathbf{I}_{Mn}$ to $\mathbf{M}_{Mn}$ in weakly donating solvents to the relative donor properties of those media clearly points to the importance of solvent stabilization of the transition state for methyl migration. The relative effectiveness in this respect correlates qualitatively with the donor properties even for these solvents and suggests direct interaction with the metal center in the transition state of the k_M pathway.

A recent report [24] of theoretical computations based upon density functional calculations has drawn some sweeping conclusions that intermediates in the thermal and photochemical pathways are different, and that neither **C** nor **S** represent intermediates in the former mechanism. Instead, the conclusion was drawn that the reactive intermediate important to the thermal reaction of $\mathbf{M}_{Mn}$ with CO is the agostic complex **B**, which reacts directly with CO to give the acyl product $\mathbf{A}_{Mn}$. The calculations agree that among species with the 'unsaturated' formulation $Mn(CO)_4(C(O)Me)$, **C** is substantially lower in energy than **B**, but suggest the barrier to forming **C** is large. Surprisingly, the calculations suggest **B** to lie in a potential energy minimum so shallow (0.1 kcal M^{-1}) that it can hardly be considered a reactive intermediate, since this is considerably less than kT (0.6 kcal M^{-1}) at ambient temperature. Steady state kinetics treatment of such a species would be inappropriate. Fig. 6 is an illustration of the lowest energy pathway calculated for the direct reaction of CO

with $\mathbf{M}_{Mn}$ to give $\mathbf{A}_{Mn}$ via formation of **B** drawn appropriately to scale according to the calculations. Although the issue was not raised by the authors of that report, this reaction coordinate profile is essentially one of a concerted reaction, i.e. the k_3 pathway in Scheme 1.

In previous experimental kinetics studies [9,25], the reaction of **M** with L in alkane solutions proved to be strictly second order over the ligand concentrations studied. While this is consistent with a direct nucleophilic attack via the k_3 step in these weaker donor solvents, a kinetically consistent alternative would be reaction via formation of $\mathbf{I}_{th}$, if the constraint $k_{-1} \gg k_2[L]$ were met under the experimental conditions. The photochemically derived rate constants for **I** in cyclohexane clarify this ambiguity. The condition $k_M \gg k_L[L]$ is not met for the reaction of **M** with excess $P(OMe)_3$ in cyclohexane ($k_M = 9.0\ s^{-1}$, $k_L = 1.4 \times 10^6\ M^{-1}\ s^{-1}$, [L] = 0.006–0.15 M) [9]. Thus, the most plausible explanation of the second order kinetics in alkanes is that the reaction proceeds via the k_3 step, presumably involving associative attack of L on the Mn, although a less direct pathway such as nucleophilic activation of a carbonyl is difficult to exclude [26,27]. In more polar solvents where there is kinetics evidence for an intermediate, the overall rates are much faster, consistent with the role of solvent in assisting alkyl migration.

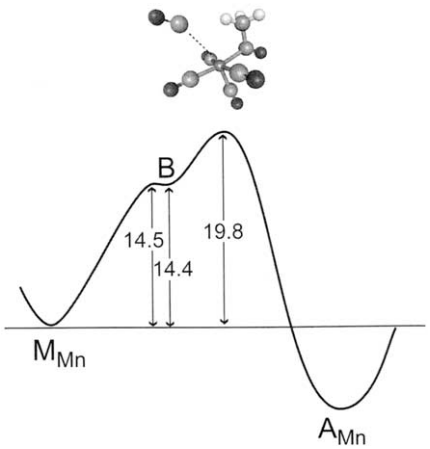

Fig. 6. A (to scale) drawing of the reaction profile calculated by DFT techniques [24] for the concerted reaction of CO with $\mathbf{M}_{Mn}$ to give $\mathbf{A}_{Mn}$ via the agostic configuration **B**, was calculated to have a potential minimum ~0.1 kcal M^{-1} deep.

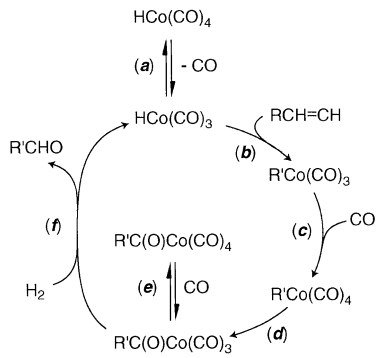

Scheme 2. Proposed mechanism for homogeneous cobalt-catalyzed hydroformylation.

3.2. Cobalt carbonyl catalysts

Carbonylation catalysis has grown to be a major component of the chemical industry since the discovery of homogeneous cobalt carbonyl catalysts for alkene hydroformylation in 1938 by Otto Roelen at Ruhrchemie AG [1,2]. The original hydroformylation catalysts were based on simple cobalt carbonyl precursors; however, a phosphine modified cobalt carbonyl catalyst has been developed, which has a more favorable linear-to-branched selectivity, but requires higher temperatures for desirable activity. In the early 1960s, Heck and Breslow proposed the generally accepted catalytic cycle for unmodified cobalt catalysts illustrated in Scheme 2 [28], and a similar model can be presumed for the phosphine modified system. Described here are TRIR studies of the reactive intermediates in migratory insertion of a CO into the Co–R bond of the phosphine modified complex $RC(O)Co(CO)_3L$.

Thermal kinetics studies on $RC(O)Co(CO)_3L$ (R, alkyl; L, CO, phosphine) using in situ IR [29,30] and NMR [31,32] techniques have reported inverse dependence upon [CO] for the rates of CO exchange, reaction with H_2, and isomerization of R. The unsaturated intermediate $RC(O)Co(CO)_2L$ has been invoked in mechanism discussions, but these techniques could not probe the spectra or dynamics of this species directly. For example, Roe used high pressure NMR magnetization exchange experiments [32] to determine activation parameters for CO loss from $CH_3C(O)Co(CO)_4$ ($\mathbf{A}'_{Co}$) in methylcyclohexane-d_{14} as $\Delta H^{\ddagger} = 22$ kcal M^{-1}, $\Delta S^{\ddagger} = 8$ cal $M^{-1}\ K^{-1}$ and suggested that the transition state for CO dissociation involved concerted coordination of the acyl oxygen to give the η^2-acyl intermediate. Indeed, there is spectroscopic evidence that supports the stabilization of $\mathbf{I}'_{Co}$ via coordination with the acyl oxygen. Photodecarbonylation of $\mathbf{A}'_{Co}$ in argon matrices [33,34] demonstrated the formation of a species formulated as $\mathbf{I}'_{Co}$, and Sweany attributed the diminished intensity of the acyl ν_{CO} band to a cyclic η^2 conformation for the acyl group. Under these conditions, $\mathbf{I}'_{Co}$ was remarkably stable even in the presence of CO and H_2, whereas the methyl and hydride analogs $CH_3Co(CO)_3$ and $HCo(CO)_3$ (from photolysis of the methyl and hydrido tetracarbonylcobalt complexes, respectively) both reacted readily with CO and H_2. Density functional calculations on reactive intermediates of the unmodified cobalt catalyzed hydroformylation cycle by Ziegler et al. [35–37] also predict the η^2 acyl structure (**C′**) for $CH_3C(O)Co(CO)_3$ as the most stable conformation for $\mathbf{I}'_{Co}$.

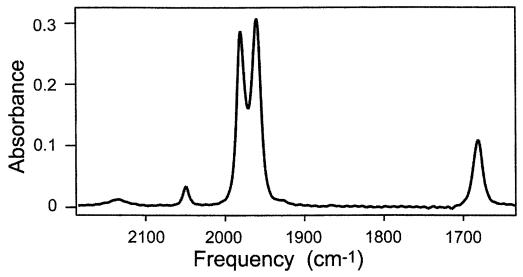

Fig. 7. Infrared spectrum of a 2.14 mM solution of $CH_3C(O)Co(CO)_3PPh_3$ ($\mathbf{A}_{Co}$) in benzene-d_6 under 1 atm of carbon monoxide. The peak positions are 1680 cm^{-1} for the acyl CO, 1959, 1979, 2048 cm^{-1} for the terminal CO, and 2131 cm^{-1} for free CO in solution.

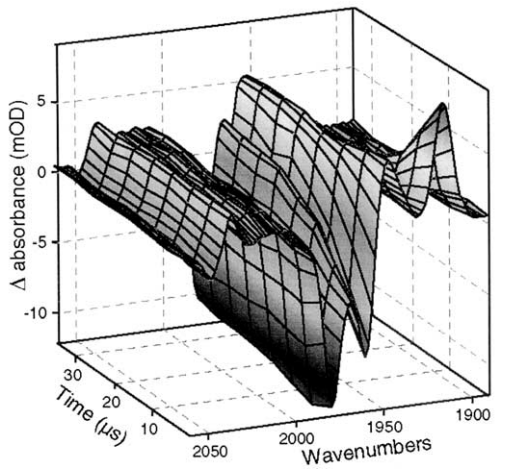

Fig. 8. Infrared transient difference spectra of $CH_3C(O)Co(CO)_3PPh_3$ ($\mathbf{A}_{Co}$) in C_6D_6 recorded 0–35 μs following the laser pulse.

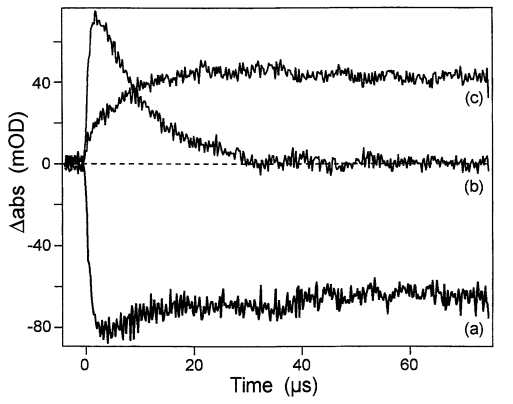

Fig. 9. The absorption changes following 355 nm flash photolysis of $CH_3C(O)Co(CO)_3PPh_3$ ($\mathbf{A}_{Co}$) in C_6D_6 monitored at, (a) 1979 cm^{-1} corresponding to the bleach of $\mathbf{A}_{Co}$, (b) 1915 cm^{-1} due to the absorption of the transient intermediate $\mathbf{I}_{Co}$, and (c) 1958 cm^{-1} showing the formation of the methyl complex $\mathbf{M}_{Co}$ [14].

In this laboratory, solution studies [14] of the 355 nm photolysis of the phosphine modified cobalt carbonyl $CH_3C(O)Co(CO)_3PPh_3$ ($\mathbf{A}_{Co}$) have probed the spectra and reactivity of the unsaturated intermediate $CH_3C(O)Co(CO)_2PPh_3$ ($\mathbf{I}_{Co}$). The IR spectrum of a benzene-d_6 solution of $\mathbf{A}_{Co}$ is shown in Fig. 7. This displays a weak band at 2048 cm^{-1} and strong bands at 1979 and 1959 cm^{-1} for the terminal carbonyl stretches. This is consistent with trigonal bipyramidal coordination of the ligands perturbed from local C_{3v} symmetry by the acyl group. The acyl carbonyl stretch was observable at $\nu_{CO} = 1680$ cm^{-1}.

Insight into the events following the 355 nm photolysis of the parent complex $\mathbf{A}_{Co}$ is provided by examination of the IR spectral changes on the microsecond timescale. The surface plot of the absorbance changes following photolysis collected by stepscan FTIR detection in the terminal ν_{Co} region is shown in Fig. 8. Readily apparent spectral changes are the prompt bleach of the parent terminal CO stretches at 2048, 1979, and 1959 cm^{-1}, characteristic of depletion of $\mathbf{A}_{Co}$, and the prompt formation and decay of a transient species $\mathbf{I}_{Co}$ with initially strong absorbances at 1915 and 1947 cm^{-1}. The prompt absorbance at 1947 cm^{-1} is in a congested spectral region close to both the 1959 cm^{-1} bleach of $\mathbf{A}_{Co}$ and the growth of a 'permanent' (long lived) photoproduct that was shown to be $CH_3Co(CO)_3PPh_3$ ($\mathbf{M}_{Co}$) [14]. The decay of the absorbance at 1915 cm^{-1} is clear of any overlap of $\mathbf{A}_{Co}$ bleach or product growth.

By selecting frequency intervals corresponding to the bleach of $\mathbf{A}_{Co}$ at 1979 cm^{-1}, the transient absorbance of the intermediate $\mathbf{I}_{Co}$ at 1915 cm^{-1}, and the product formation at 1958 cm^{-1}, it is possible to generate the transient signals for these species as shown in Fig. 9. The kinetic trace of product formation at 1958 cm^{-1} fits well to an exponential rise with an observed rate constant (k_{obs}) of ca. 1.3×10^5 s^{-1}. This value is in agreement with the k_{obs}, (1.2×10^5 s^{-1}) obtained from an exponential fit of the decay of $\mathbf{I}_{Co}$ at 1915 cm^{-1}, so it is reasonable to assume that $\mathbf{I}_{Co}$ reacts directly to form this photoproduct. Under these conditions, ($P_{CO} \cong 0.76$ atm) regeneration of $\mathbf{A}_{Co}$ on this timescale is at most quite modest (Fig. 9) and roughly follows the k_{obs} of the photoproduct and $\mathbf{I}_{Co}$.

The spectrum of the intermediate(s) formed promptly ($\mathbf{I}_{Co}$) can be extracted from the difference spectrum first 1.5 μs after the pump laser pulse and shows strong bands at 1915 and 1947 cm^{-1} plus weaker ones at 2035 and 1983 cm^{-1}. The shift of the terminal ν_{CO} to 1915 and 1947 cm^{-1} is consistent with CO loss being the primary photoprocess, although manipulations of the step-scan spectral data leave some doubt as to whether the minor product $CH_3C(O)Co(CO)_3$ is also formed by phosphine photodissociation. This should have higher frequency ν_{CO} bands consistent with the observation of weaker bands at 2035 and possibly 1983 cm^{-1} in the step-scan spectra (Fig. 10). However, no indication of sample degradation was detected in the IR spectra of the photolysis solutions, and small concentrations of

I'_{Co} should not affect the kinetics of $\mathbf{I}_{Co}$ measured at 1915 cm^{-1}. The results of the subtractions of transient IR spectra are all consistent with the scenario illustrated in Scheme 3; photolysis of the acetyl complex $\mathbf{A}_{Co}$ at 355 nm gives a reactive intermediate $\mathbf{I}_{Co}$, which reacts further to give $\mathbf{M}_{Co}$ or to reform $\mathbf{A}_{Co}$.

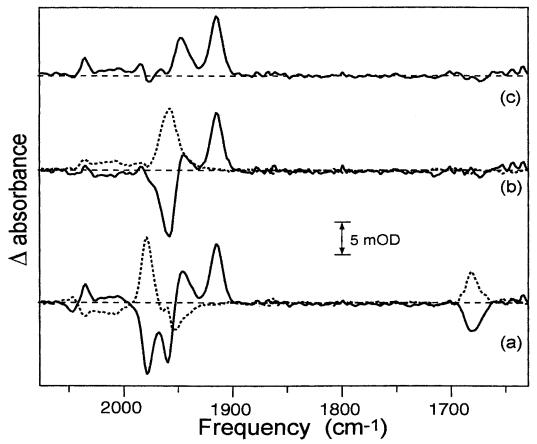

Fig. 10. (a) Transient difference spectrum extracted from the first 1.5 μs following 355 nm photolysis of $CH_3C(O)Co(CO)_3PPh_3$ ($\mathbf{A}_{Co}$) in C_6D_6 (solid line) and the negative of the transient difference spectrum for the time period from 40 to 80 μs (dashed line). (b) The resultant spectrum from the addition of the spectrum in (a) (solid line) and the weighted spectrum of $\mathbf{M}_{Co}$ (dashed line). (c) The spectrum of $\mathbf{I}_{Co}$.

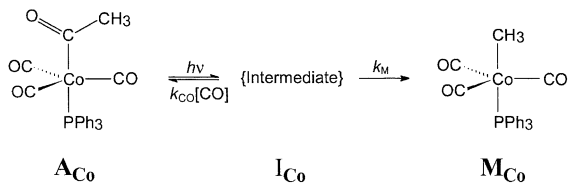

Scheme 3. Photolysis scheme for $CH_3C(O)Co(CO)_3PPh_3$.

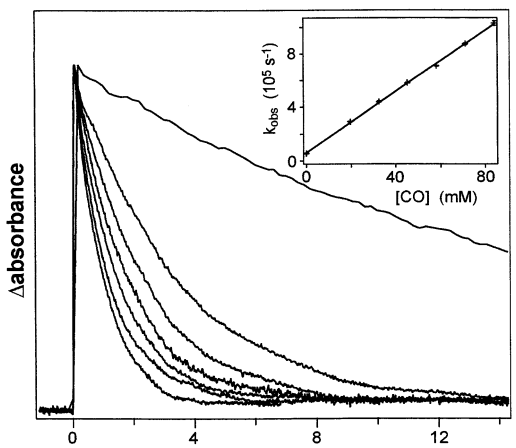

Fig. 11. Decay curves for $\mathbf{I}_{Co}$ at 1915 cm^{-1} following 355 nm flash photolysis of $\mathbf{A}_{Co}$ in benzene at 25 °C at [CO] = 0, 20, 32, 45, 58, 71, and 84 mM from top to bottom, respectively. The initial absorbance change of the individual traces were normalized. The inset graph is a plot of the k_{obs} vs. [CO] for the same data.

Table 2
Rate constants k_M and k_{CO} following 355 nm photolysis of $CH_3C(O)Co(CO)_3PPh_3$ in benzene at 25–40 °C

T (°C)	k_M (10^4 s^{-1})	k_{CO} (10^7 M^{-1} s^{-1})
25	6.2 (±0.7)	1.14 (±0.01)
30	7.6 (±0.5)	1.19 (±0.01)
35	10.5 (±0.9)	1.26 (±0.02)
40	13.5 (±0.6)	1.34 (±0.01)
45	18.0 (±0.8)	1.40 (±0.02)
$\Delta H^{\ddagger}$ (kcal M^{-1})	9.5 (±0.5)	1.4 (±0.1)
$\Delta S^{\ddagger}$ (cal M^{-1} K^{-1})	−5 (±1.5)	−22 (±3)

Data from Ref. [14].

Shown in Fig. 11 are curves representing the decay of $\mathbf{I}_{Co}$ monitored at 1915 cm^{-1} in 25 °C benzene solutions equilibrated with various P_{CO} ranging from 0 to 11.3 atm. These P_{CO} values correspond to CO concentrations from 0 to 84 mM [33,34]. The curves can be fit as single exponential decays, the rates of which increase with [CO]. The decay of $\mathbf{I}_{Co}$ as a function of [CO] can be modeled by a simple competition between two available reaction paths, a unimolecular methyl migration with the associated rate k_M to form $\mathbf{M}_{Co}$; and a bimolecular reaction with CO with the associated rate k_{CO} to reform $\mathbf{A}_{Co}$ (Scheme 3). For this model, $k_{obs} = k_{CO}[CO] + k_M$. Accordingly, a plot of k_{obs} versus [CO] is linear (Fig. 6 inset) with slope $k_{CO} = 1.14 (\pm 0.01) \times 10^7$ M^{-1} s^{-1} and non-zero intercept $k_M = 6.2 (\pm 0.7) \times 10^4$ s^{-1}.

The activation parameters $\Delta H^{\ddagger}$ and $\Delta S^{\ddagger}$ for the two competitive pathways of $\mathbf{I}_{Co}$, k_{CO} and k_M, were determined from kinetics for the decay of $\mathbf{I}_{Co}$ in benzene observed over the temperature range 25–45 °C in 5 °C increments. These data are summarized in Table 2. Plots of k_{obs} versus [CO] were observed to be linear at each temperature, and both the k_{CO} and k_M increase with T. However, the temperature sensitivity of the k_{CO} pathway is very slight ($\Delta H^{\ddagger}_{CO} = 1.4 \pm 0.1$ kcal M^{-1}), while that of the k_M pathway is much larger ($\Delta H^{\ddagger}_{M} = 9.5 \pm 0.5$ kcal M^{-1}). The respective $\Delta S^{\ddagger}$ values were determined to be -22 ± 3 and -5 ± 1.5 cal M^{-1} K^{-1}, respectively.

In the context of the discussion for the manganese analogs above, the 'unsaturated' species $\mathbf{I}_{Co}$ can be discussed in terms of three potential structures, the cyclic η^2-acyl complex **C**, the solvent stabilized species **S**, or the bidentate β-agostic complex **B**. The negative entropies of activation for both k_M and k_{CO} (−5 and −22 cal M^{-1} K^{-1}, respectively) indicate that, in benzene, neither pathway is dominated by a rate limiting step involving solvent dissociation. Furthermore, the insensitivity of k_{CO} to the solvents (Table 3) points toward $\mathbf{I}_{Co}$ being stabilized by means other than adoption of the **S** configuration.

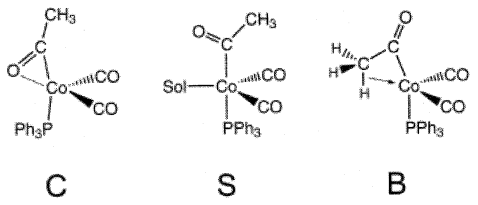

Spectral and kinetic data support the assignment of a η^2-chelated **C** configuration for $\mathbf{I}_{Co}$. A transient difference spectrum of the acyl region displayed bleaching of $\mathbf{A}_{Co}$ acyl ν_{CO}, and a weaker absorbance shifted to 41 ± 2 cm^{-1} to lower the energy, both following the same kinetics as observed for the terminal ν_{CO} absorbance changes. The reduced spectral intensity and shift is in accordance with other observed η^2-acyl complexes [38]. Notably, the terminal ν_{CO} shifts between the IR spectrum of $CF_3C(O)Co(CO)_3PPh_3$ ($\mathbf{A}_F$) and the TRIR spectrum of $\mathbf{I}_F$ believed to be solvent stabilized **S** in DCE are similar, but the shift in the acyl ν_{CO} in that case (16 ± 3 cm^{-1}) is much smaller (in the case of $\mathbf{I}_F$, the, reactivity towards CO in dichloromethane is an order of magnitude higher than for $\mathbf{I}_{Co}$ [9]). A bidentate **B** conformation for $\mathbf{I}_{Co}$ is furthermore unlikely due to the failure to observe the predicted inverse kinetic isotope effect for the disruption of the interaction with the CH_3 of $\mathbf{I}_{Co}$ in experiments on $CD_3C(O)Co(CO)_3PPh_3$ [39]. Such observations are consistent with, yet do not prove, the assignment of $\mathbf{I}_{Co}$ as having the **C** conformation.

Table 3
Rate constants for methyl migration, k_M and for reaction with CO, k_{CO} following 355 nm photolysis of $CH_3C(O)Co(CO)_3PPh_3$ in various solvents at 25 °C

Solvent	k_M (10^5 s^{-1})	k_{CO} (10^6 M^{-1} s^{-1})
THF	12 ± 0.4	7.8 ± 0.5
Benzene	0.62 ± 0.07	11.4 ± 0.1
Dichloromethane	1.9 ± 0.2	16 ± 1
Dichloroethane	3.5 ± 0.2	10 ± 0.8

Data from Ref. [14].

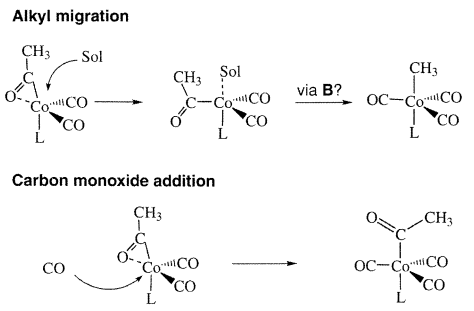

Scheme 4.

The ability of the acyl ligand to participate in either an η^2-acyl **C** or β-agostic **B** fashion directly affects the reactivity of unsaturated cobalt acyl complexes. To this end, studies are in progress on the sensitivity of k_{CO} and k_M to the nature of the acyl ligand ($CH_3CH_2(O)Co(CO)_3PPh_3$ $\mathbf{A}_{Et}$) and that of the phosphine ($CH_3C(O)Co(CO)_3P(n\text{-}Bu)_3$; $\mathbf{A}_{PBu_3}$). The results of these preliminary TRIR photolysis experiments confirm the formation of a CO loss intermediate species $\mathbf{I}_{Et}$ and $\mathbf{I}_{PBu_3}$, that exhibit a marked change in reactivity towards CO and methyl migration. The values for k_{CO} and k_M measured for $\mathbf{I}_{Et}$ at 25 °C in benzene solution are both significantly reduced from those of $\mathbf{I}_{Co}$, while $\mathbf{I}_{PBu_3}$ also exhibits a lower k_{CO}, yet a tenfold increase in k_M.

4. Summary

A generalized model for the intermediates prepared by photodissociation of CO from the cobalt and manganese complexes $\mathbf{A}_{Co}$ and $\mathbf{A}_{Mn}$ is that the intermediate **I** can be considered an equilibrium ensemble of the three species **C**, **S** and **B** from which methyl migration to form **M** or trapping with CO to form **A** occurs. For studies of $\mathbf{A}_{Co}$, the TRIR spectra are consistent with **C** being the most prevalent configuration of $\mathbf{I}_{Co}$ even in the strong donor solvent THF, unlike $\mathbf{I}_{Mn}$. That $\mathbf{I}_{Co}$ is not **S**, is substantiated by the insensitivity of k_{CO} to solvent donor properties, suggesting a simple concerted displacement of the η^2-acyl oxygen by CO. This view is substantiated by the large negative $\Delta S^{\ddagger}$ of that step in benzene solution. In contrast, k_M is dependent on the solvent medium in a manner suggestive of an intimate role of solvent in the methyl migration. This may simply reflect the necessity of solvent association to facilitate the isomerization of **C** to **B**, placing the CH_3 in a stereochemical location more favorable for migration, Scheme 4 illustrates mechanisms for these steps consistent with the various observations.

In these contexts, the behavior of $\mathbf{I}_{Co}$ parallels that of the manganese analog $\mathbf{I}_{Mn}$ with the exception that for the latter in THF, the solvated configuration is apparently dominant. Another key difference is the much greater reactivity of the cobalt complexes which are about four orders of magnitude faster for both the CO addition and the methyl migration rates. Thus, the manganese carbonyls appear to provide a reasonable model for migratory insertion processes of the cobalt catalysts; however, it is the much greater reactivities of cobalt carbonyls that make these viable as practical carbonylation catalysts.

Acknowledgements

This research was sponsored by a grant (DE-FG03-85ER13317) to PCF from the Division of Chemical Sciences, Office of Basic Energy Sciences, US Department of Energy. Some laser flash photolysis experiments were carried out on a time resolved optical system constructed with support from a US Department of Energy University Research Instrumentation Grant (No. DE-FG05-91ER79039). Recent contributors in this laboratory to the experimental time resolved spectroscopic studies relevant to those discussed here include: Brian Lee, Karen McFarlane, Bill Boese, David Ryba, Jon Marhenke, Torsten Buttner, Verena Mertins, Julie G. Rabor, and Stefan Elbers. Stefan Bernhard and Jon R. Schoonover, collaborators at Los Alamos National Laboratory, also made important contributions.

References

[1] G.W. Parshall, S.D. Ittle, Homogeneous Catalysis, second ed., Wiley-Interscience, New York, 1992 Chapter 5.
[2] B. Cornils, W.A. Herrmann, Applied Homogeneous Catalysis With Organometallic Compounds: A Comprehensive Handbook in Two Volumes, VCH, Weinheim/New York, NY, USA, 1996.
[3] D. Wink, P.C. Ford, J. Am. Chem. Soc. 107 (1985) 1794.
[4] D. Wink, P.C. Ford, J. Am. Chem. Soc. 109 (1987) 436.
[5] J.A. DiBenedetto, D.W. Ryba, P.C. Ford, Inorg. Chem. 28 (1989) 3503.
[6] S.T. Belt, D.W. Ryba, P.C. Ford, J. Am. Chem. Soc. 113 (1991) 9524.
[7] W.T. Boese, B.L. Lee, D.W. Ryba, S.T. Belt, P.C. Ford, Organometallics 12 (1993) 4739.
[8] W.T. Boese, P.C. Ford, Organometallics 13 (1994) 3525.
[9] W.T. Boese, P.C. Ford, J. Am. Chem. Soc. 117 (1995) 8381.
[10] J.S. Bridgewater, B. Lee, S. Bernhard, J.R. Schoonover, P.C. Ford, Organometallics 16 (1997) 5592.
[11] K.L. McFarlane, P.C. Ford, Organometallics 17 (1998) 1166.
[12] K.L. McFarlane, B. Lee, W.F. Fu, R. van Eldik, P.C. Ford, Organometallics 17 (1998) 1826.
[13] S.M. Massick, P.C. Ford, Organometallics 18 (1999) 4362.
[14] S. Massick, J. Rabor, S. Elbers, J. Marhenke, S. Bernhard, J. Schoonover, P.C. Ford, Inorg. Chem. 39 (2000) 3098.
[15] J.S. Bridgewater, J.R. Schoonover, T.L. Netzel, S.M. Massick, P.C. Ford, Inorg. Chem. 41 (2001) 1466.
[16] P.C. Ford, J.S. Bridgewater, B. Lee, Photochem. Photobiol. 65 (1997) 57.
[17] S.P. Church, H. Herman, F.-W. Grevels, K. Schaffner, Inorg. Chem. 24 (1985) 418.
[18] J.J. Turner, M.W. George, I.P. Clark, I.G. Virrels, Laser Chemistry 19 (1999) 245 and references therein.
[19] (a) A. Lugovskoy, R. Paur-Afshari, R.H. Schultz, J. Phys. Chem. 104 (2000) 10587;
(b) G.T. Long, E. Weitz, J. Am. Chem. Soc. 122 (2000) 1431 and references therein.
[20] J.P. Collman, L.S. Hegedus, J.R. Norton, R.G. Finke, Principles and Applications of Organotransition Metal Chemistry, University Science Books, Mill Valley, CA, 1987 Chapter 6.
[21] J. Marhenke, V. Reyes, studies in progress.
[22] (a) G.K. Yang, V. Vaida, K.S. Peters, Polyhedron 7 (1988) 1619;
(b) J. Morse, G. Parker, T.J. Burkey, Organometallics 8 (1989) 2471.
[23] G. Ujaque, F. Maseras, A. Lledos, L. Contreras, A. Pizzano, D. Rodewald, L. Sanchez, E. Carmona, A. Monge, C. Ruiz, Organometallics 18 (1999) 3294.
[24] Derecskei-Kovacs, D.S. Marynick, J. Am. Chem. Soc. 122 (2000) 2078.
[25] R.J. Mawby, F. Basolo, R.G. Pearson, J. Am. Chem. Soc. 86 (1964) 3994.
[26] P.C. Ford, A. Rokicki, Adv. Organomet. Chem. 28 (1988) 139.
[27] S. Webb, C. Giandomenico, J. Halpern, J. Am. Chem. Soc. 108 (1986) 345.
[28] R.F. Heck, D.S. Breslow, J. Am. Chem. Soc. 83 (1961) 4023.
[29] I. Kovacs, F. Ungvary, L. Marko, Organometallics 5 (1986) 209.
[30] P. Pino, A. Major, F. Spindler, R. Tannenbaum, G. Bor, I.T. Horvath, J. Organomet. Chem. 417 (1991) 65.
[31] J.W. Rathke, R.J. Klinger, T.R. Krause, Organometallics 10 (1991) 1350.
[32] D.C. Roe, Organometallics 6 (1987) 942.
[33] R.L. Sweany, Organometallics 8 (1988) 175.
[34] R.L. Sweany, F.N. Russell, Organometallics 7 (1988) 719.
[35] L. Versluis, T. Ziegler, E.J. Baerends, W. Ravenek, J. Am. Chem. Soc. 111 (1989) 2018.
[36] L. Versluis, T. Ziegler, Organometallics 9 (1990) 2985.
[37] M. Sola, T. Zeigler, Organometallics 15 (1996) 2611.
[38] A.R. Hermes, G.S. Girolami, Organometallics 7 (1987) 394.
[39] S.M. Massick, T. Büttner, P.C. Ford, in preparation.